Effect of Three-Dimensional Structure on the Stormwide Horizontal Accelerations and Momentum Budget of a Simulated Squall Line

STANLEY B. TRIER, MARGARET A. LEMONE, AND WILLIAM C. SKAMAROCK

National Center for Atmospheric Research, Boulder, Colorado*

(Manuscript received 17 July 1997, in final form 11 December 1997)

ABSTRACT

Past studies of the effects of mesoscale convective systems (MCSs) on the environmental flow have been limited by data coverage and resolution. In the current study the MCS-scale (stormwide) horizontal accelerations and momentum budget associated with an oceanic MCS are analyzed using output from a high-resolution three-dimensional numerical model integrated over a large domain. The simulation is based on an observed MCS that occurred on 22 February 1993 during the Tropical Ocean Global Atmosphere Coupled Ocean–Atmosphere Response Experiment. An important aspect of both the observed and simulated MCS is its evolution from a quasi-two-dimensional to an asymmetric three-dimensional morphology, which was demonstrated in companion studies to result from the finite length of the MCS interacting with environmental vertical shear that varies in direction with height. Herein, the authors focus on the effects of the three-dimensional structure on MCS-scale horizontal accelerations.

The horizontal accelerations over the central portion of the MCS, where its leading edge is perpendicular to the low-level environmental vertical shear, resemble those from available observations and two-dimensional models of linear squall-type MCSs. However, the vertical structure of horizontal accelerations is quite different on the MCS scale. Zonal accelerations, which are aligned along the environmental low-level vertical shear, generally exceed meridional accelerations in the lower and upper troposphere, and are dominated by the vertical flux convergence term at low levels, and by the horizontal flux convergence term at upper levels. In contrast, zonal accelerations are weaker than meridional accelerations at midlevels, owing to strong cancellation of zonal accelerations in the central portion with those along the northern periphery of the MCS, where both the alignment of the convective band relative to the environmental vertical shear and its mesoscale organization are different. This compensation between different regions of the MCS results in modifications to the environmental vertical shear by mesoscale convection that differ substantially from those typically reported in idealized studies of two-dimensional squall lines. Since three-dimensional organization often occurs in MCSs that lack persistent external linear forcing, the current findings may have implications for the parameterization of the momentum effects of mesoscale deep convection in large-scale models.

1. Introduction

Mesoscale convective systems (MCSs) represent a form of organized deep atmospheric convection on scales of ~100 km or greater (e.g., Houze 1993, 334). In addition to producing significant local weather, MCSs play an important role in the redistribution of heat, moisture, and momentum in the global atmosphere. This may be particularly true over the warm waters of the equatorial western Pacific Ocean, where organized deep convection is frequent and often widespread.

Using shipboard radar data, Rickenbach and Rutledge (1998) estimated that 75% of the rainfall that occurred during the Tropical Ocean Global Atmosphere (TOGA) Coupled Ocean–Atmosphere Response Experiment (COARE)[1] was associated with precipitation systems organized on scales of 100 km or greater. Nearly half of the MCS-scale events examined by Rickenbach and Rutledge displayed the linear organization often found in squall-type systems (e.g., Newton 1950; Zipser 1977), which are characterized by rapid movement and the most intense rainfall within a narrow band at their leading edge. In the current study we examine the system-scale horizontal accelerations and momentum budget of a squall-type MCS that occurred on 22 February 1993 during TOGA COARE.

Although organized deep convection may signifi-

* The National Center for Atmospheric Research is sponsored by the National Science Foundation.

Corresponding author address: Dr. Stanley B. Trier, National Center for Atmospheric Research, P.O. Box 3000, Boulder, CO 80307-3000.
E-mail: trier@ncar.ucar.edu

[1] The objectives of TOGA COARE, which was conducted over the western equatorial Pacific Ocean from November 1992 until March 1993, are summarized by Webster and Lukas (1992).

© 1998 American Meteorological Society

cantly influence generation and redistribution of horizontal momentum in the atmosphere, computational limitations preclude its explicit simulation in current general circulation models (GCMs), operational forecast models, and most mesoscale models. However, observational (e.g., Barnes and Sieckman 1984; Alexander and Young 1992) and numerical (e.g., Weisman and Klemp 1986) studies have established that resolvable-scale characteristics of the environment, such as the vertical wind shear and buoyancy, are significant factors governing the intensity, organization, and evolution of deep convection. If the orientation and evolution of mesoscale convection could be predicted, the results could be used to improve understanding of the relationship between convective organization and the modifications to the environment, which in turn could potentially lead to improvements in the parameterization of the effects of MCSs in large-scale models.

There are currently no general theories that describe the effects of deep convection on the large-scale distribution of horizontal momentum. However, idealized analytic models (Moncrieff 1981, 1992) have demonstrated ability in reproducing characteristics of the momentum transport in mature MCSs exhibiting highly two-dimensional organization (LeMone and Moncrieff 1994). For instance, the Moncrieff (1992) model predicts that mesoscale lines of deep convection transport line-normal horizontal momentum in such a way that accelerates flow rearward at middle and upper levels and forward at lower levels, as found in observations (e.g., LeMone 1983; LeMone et al. 1984; Smull and Houze 1987). The significance of this momentum transport is that it can systematically enhance the vertical shear in the direction opposite to which the precipitation system is moving.

Studies of momentum budgets of MCSs have, however, shown that several competing effects determine how deep convection modifies the flow. Results based on radar observations (e.g., Smull and Houze 1987; Lafore et al. 1988; Lin et al. 1990; LeMone and Jorgensen 1991; Hane and Jorgensen 1995) and numerical simulations (e.g., Lafore et al. 1988; Gao et al. 1990; Caniaux et al. 1995; Yang and Houze 1996) indicate that the magnitude of the areally averaged accelerations are generally much smaller than that of individual forcing terms, including the vertical convergence of the vertical flux of horizontal momentum. Moreover, recent two-dimensional simulations within large domains that resolve deep convection (e.g., Yang and Houze 1996) indicate that the momentum budget over the broad trailing stratiform region can be considerably different from that of the leading convective region of squall-type MCSs and that no single process in a particular portion of the MCS dominates the large-scale budget.

Furthermore, MCSs can be highly three-dimensional[2] when viewed on the scale of the entire precipitation system, even when they are locally well described by two-dimensional squall line dynamics (e.g., Rotunno et al. 1988) and have areally averaged properties over sub-MCS-scale regions that fit within this conceptual paradigm. Systematic spatial variations in both convective structure and the associated mesoscale horizontal flow along the length of the MCS frequently accompanies three-dimensionality. This variation in mesoconvective organization is expected when there is horizontal variation in the pre-MCS environment (e.g., Smull and Augustine 1993; Hane and Jorgensen 1995). Three-dimensional numerical simulations have indicated that such variation can also occur in finite-length MCSs that develop in initially horizontally homogeneous environments and are influenced by Coriolis accelerations (Skamarock et al. 1994) or directional vertical shear in the environment (Trier et al. 1997). Indeed, such influences may partly explain the common observation of the evolution of MCSs toward an asymmetric structure (e.g., Loehrer and Johnson 1995). Despite the apparent frequency of three-dimensional structure (e.g., Houze et al. 1990; Blanchard 1990), its importance to horizontal accelerations averaged over the MCS scale is, as yet, unclear since past observational and numerical studies have been either constrained by idealized two-dimensional geometry, inadequate resolution of deep convective motions, or domains that do not encompass the entire precipitation system.

Herein, we address this gap in current knowledge by using a three-dimensional cloud-resolving simulation over a large domain to directly examine the combined effect of three-dimensionality and the associated variability in mesoconvective structure in a squall-type MCS on stormwide horizontal accelerations. In section 2, we briefly describe the numerical model used to simulate deep convection and discuss conditions observed in the environment of the MCS selected for simulation. The observed (Jorgensen et al. 1997) and simulated (Trier et al. 1996, 1997) MCS evolved from a quasi-linear to a three-dimensional asymmetric structure in a similar manner. A synopsis of this evolution is provided in section 3. Areally averaged vertical motions and momentum fluxes in distinct subregions of the MCS are presented in section 4. These sub-MCS-scale calculations aid in the interpretation of the stormwide horizontal accelerations and momentum budget presented in sections 5 and 6, respectively, and can be directly compared with analyses over limited portions of MCSs from previous studies. We focus our analysis in sections 5 and 6 on the period during which the MCS attains three-dimensional structure and find that while a portion of the MCS exhibits horizontal accelerations that resemble those of idealized two-dimensional squall lines, the accelerations on the scale of the entire MCS can be substantially different. Results are summarized in section 7, where some implications of our findings are dis-

[2] We use the terminology "three-dimensional" (in the current context of squall-type systems) to refer to system-scale departures from linear geometry of the MCS leading-edge convective zone.

cussed within the context of efforts to parameterize the effects of organized convection in large-scale models.

2. Environmental conditions and numerical model

Deep convection is simulated for 6 h using a three-dimensional nonhydrostatic primitive equation model that employs the automated adaptive grid algorithms described in Skamarock (1989) and Skamarock and Klemp (1993). These multiple overlapping horizontal grids enable simulations that resolve convective-scale motions within a large (540 km × 540 km) horizontal domain. The horizontal grids have spacings of 9, 3, and 1 km. The 1-km fine grids are activated by a vertical velocity threshold in regions of deep convection. All grids are stretched in the vertical so that Δz varies from 100 m at the surface to a constant value of 700 m 8 km above mean sea level (MSL). Because of the relatively short duration of the simulation and the location of the observed MCS at low latitudes (9°–10°S), neither Coriolis nor radiative effects are included. The version of the model used in this simulation contains a bulk microphysical parameterization (Rutledge and Hobbs 1984) that includes a three-class (graupel, snow, and cloud ice) ice scheme. The effects of MCS-induced surface fluxes of heat, moisture, and momentum are also represented. A more detailed description of these and other physical parameterizations, the model domain, and boundary conditions is provided in Trier et al. (1996).[3]

The environment in advance of the MCS is similar to conditions found ahead of previously documented fast-moving tropical squall lines (e.g., Barnes and Sieckman 1984). The vertical thermodynamic structure (Fig. 1a) is conditionally unstable with convective available potential energy (CAPE) of ~1500 J kg^{-1} for irreversible pseudoadiabatic ascent of a surface-based air parcel averaged through the lowest 50 mb. While moderate CAPE exists, it is distributed through a deep tropospheric layer with only modest thermal buoyancy (0°C $\leq \Delta T \leq$ 3°C) for ascending undiluted boundary layer air parcels between their levels of free convection and neutral buoyancy. The environmental hodograph (Fig. 1b) features a 12 m s^{-1} jet at 2 km MSL. The jet profile leads to substantial low-level vertical shear normal to the orientation of a significant portion of the leading edge of the MCS with weak reverse vertical shear above the jet axis. The general importance of low-level vertical shear in squall line organization has been widely established [see, e.g., Rotunno et al. (1988) for a review of past work and discussion of squall-line mechanics]. In the current tropical environment of moderate low-level vertical shear but only modest buoyancy, Trier (1997) found that the reverse shear above the low-level jet is also crucial to squall-type organization.

[3] The simulation analyzed in the current paper is the control simulation (CONTRL) described in Trier et al. (1996).

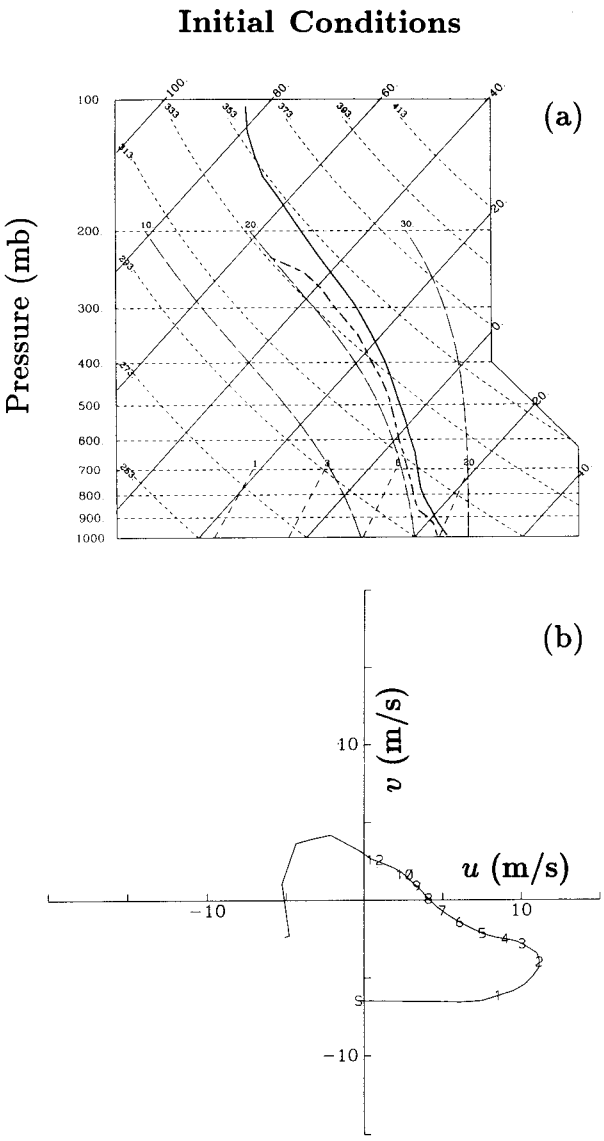

FIG. 1. (a) Temperature (solid) and dewpoint (dashed) curves in °C, and (b) hodograph (m s^{-1}) used to specify the initial condition in the numerical model. In (b), the annotations along the hodograph indicate heights in km MSL.

Deep convection is initiated in the numerical simulation by placing a finite surface-based cold pool at t = 0 in the otherwise horizontally homogeneous model domain specified by the environmental sounding (Fig. 1). A detailed explanation of both the data sources used to construct the environmental sounding and the cold pool initialization procedure is provided in Trier et al. (1996).

3. MCS structure and evolution

The evolution of the precipitation and flow structure of the simulated MCS compares well with observations (Trier et al. 1996). MCS organization mechanisms are discussed in Trier et al. (1997). In this section we pro-

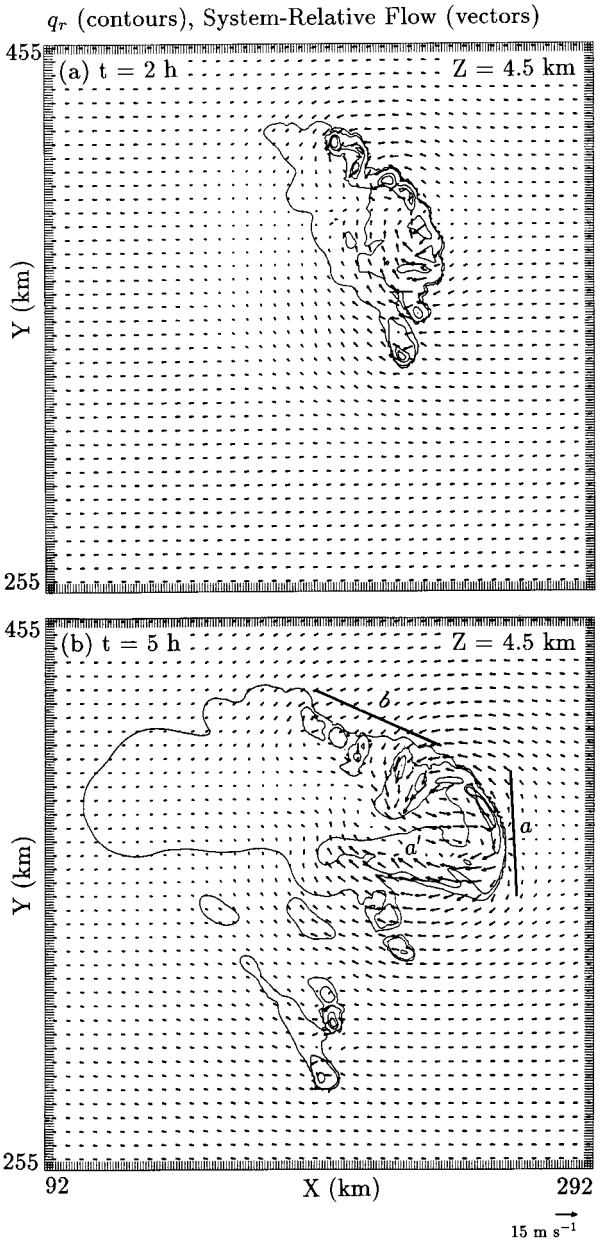

FIG. 2. The 4.5-km MSL rain field (0.01, 1, 2, 3, and 4 g kg^{-1} contours) and system-relative wind vectors over the 200 km × 200 km MCS-scale domain at (a) 2 h and (b) 5 h. In (b), the annotations indicate the precipitation features referred to in the text.

vide an overview of aspects of MCS structure and evolution that are most germane to effects on the system-scale flow.

The simulated MCS evolves from a quasi-linear band of convective precipitation into an asymmetric three-dimensional pattern with stratiform precipitation, which expands rearward from the leading convective zone between 2 and 5 h (Fig. 2). An important aspect of the three-dimensional evolution is the development of a bow-shaped segment of deep convection near the central portion of the MCS. The development of the bow echo (Fujita 1978) is associated with the growth in scale of the low- to midlevel circulations around its northern and southern edge (Fig. 2). Weisman (1993) found similar counterrotating vortices in simulations of deep convection in midlatitude environments, with greater thermodynamic instability than present in the current tropical case, when strong vertical shear was confined to the lower troposphere.

During the asymmetric stage, the leading edge of the MCS consists of dynamically distinct precipitation bands with different orientations (Fig. 2b). The central portion of the MCS leading edge (band *a*) is oriented north–south, nearly normal to the low-level vertical shear (cf. Fig. 1b). At the southern end of this band there is an appendage of weaker precipitation (denoted by *a′*) oriented transverse to the leading edge. This transverse band is fed by low-level inflow from ahead (east) of the MCS. This inflow rises abruptly in the convective updraft zone at the leading edge and is accelerated rapidly rearward along the band at midlevels (Trier et al. 1997, their Fig. 14a) in association with a portion of the southern vortex circulation depicted in Fig. 2b. In contrast, the band of more cellular deep convection (band *b*) located to the northwest of the northern vortex (Fig. 2b) is oriented parallel to the midlevel reverse shear above the environmental low-level jet (cf. Fig. 1b).

4. Sub-MCS-scale variability

Vertical motion and the related vertical fluxes of relative horizontal momentum are calculated at 3 h over four 35 km × 30 km subregions (Fig. 3), at which time the MCS is evolving into a three-dimensional asymmetric precipitation system. The domain size used in these calculations is chosen to assess and understand the variability of the mesoconvective-scale dynamics within different regions of the simulated MCS and also to facilitate comparison with analyses from previous studies, typically conducted over domains of similar size (e.g., Lafore et al. 1988; Lin et al. 1990; LeMone and Jorgensen 1991; Hane and Jorgensen 1995).

The sub-MCS-scale domains include 1) the leading convective zone of the bow echo in the central portion of the MCS; 2) a northern convective zone consisting of the more cellular precipitation band, which is separated from the central convective region by the northernmost of the two counterrotating midlevel vortices (Fig. 4) discussed in the previous section; 3) a region of weaker, stratiform precipitation located rearward of the leading edge of the MCS; and 4) a zone of more isolated deep convection along the southern flank of the simulated MCS. The southernmost domain, where isolated convective motions are weak and dissipate with time (Trier et al. 1996), has a less significant impact on MCS-scale accelerations than the other three sub-MCS-scale domains. Accordingly, while results from this re-

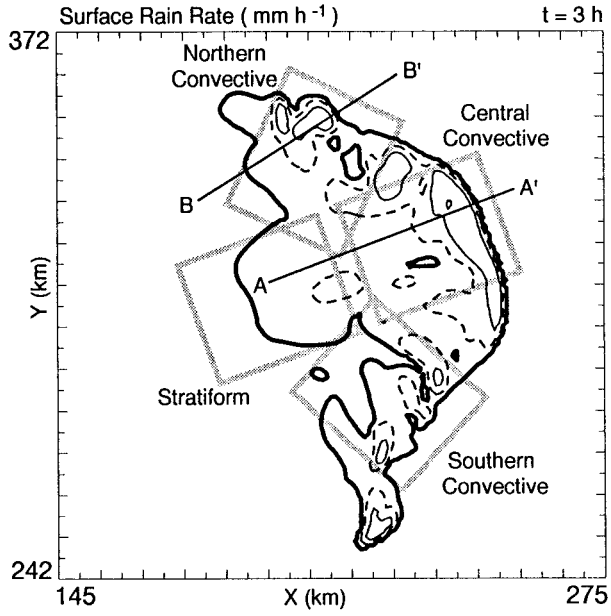

FIG. 3. Surface rain rate at 3 h contoured at 0.5 (bold, solid), 10 (dashed), and 50 mm h^{-1} (thin, solid) thresholds. The shaded rectangles represent the regional (sub-MCS-scale) domains from which areally averaged quantities that are displayed in subsequent figures are calculated. The transects *AA′* and *BB′* represent the locations of the vertical cross sections displayed in Figs. 7a and 7b, respectively.

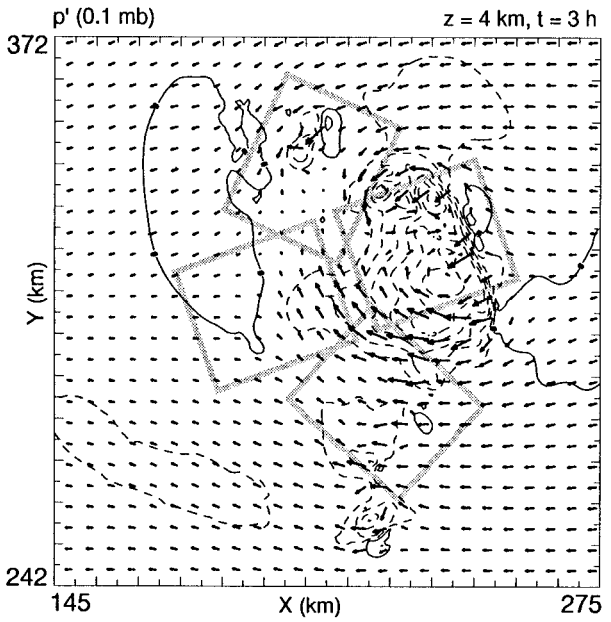

FIG. 4. The 4-km MSL pressure perturbation (0.1-mb intervals) and system-relative winds at 3 h. A vector the length of the space between tick marks has a magnitude of 10 m s^{-1}. The shaded rectangles represent the location of the regional domains as in Fig. 3. Positive values are solid; negative values are dashed.

gion are included for comparison purposes, they are not emphasized in the discussion of sub-MCS-scale variability in section 4b.

a. Methodology

Most past studies of momentum fluxes and momentum budgets associated with deep convection have been concerned with quasi-two-dimensional convective bands. The traditional analysis approach, separating the horizontal flow into components normal and parallel to the moving band, is physically based since momentum fluxes are often of different character in the band-normal and band-parallel directions (e.g., LeMone 1983).

In the current case, the leading edge of the MCS is arc shaped (Fig. 3). Nevertheless, in analyzing the sub-MCS-scale horizontal flow and momentum fluxes, it is useful, both to facilitate comparison with previous work and for the elucidation of storm dynamics, to adopt the traditional approach and decompose the horizontal flow in the northern, central, and southern convective domains into separate components that are *locally* normal and parallel to the leading edge of the MCS-induced cold pool. In addition to its orientation, the motion of the coordinate system needs to be specified in order to calculate the band-parallel and band-normal relative flow for the analysis domains. The choice of reference frame is important because the vertical fluxes of horizontal momentum and their vertical derivatives, which force the local accelerations ($\partial\overline{u}/\partial t$, $\partial\overline{v}/\partial t$) in the horizontal momentum budget equations, depend on its motion.

The reference frames chosen for the convective domains (Fig. 3) move at constant speed, approximating that of the local cold-pool edge. The most appropriate reference frame to study momentum fluxes in the stratiform domain, which is well removed from the leading edge, is less obvious. One possibility would be a reference frame that moves with the centroid of the stratiform precipitation, which expands rearward from the leading edge of the MCS with time (Fig. 2). However, trajectory analysis (not shown) reveals that much of the flow that feeds this mid-to-upper-level stratiform precipitating region originates ahead of the central convective zone and is accelerated strongly rearward while passing through the convective zone. Since the intensifying mesoscale flows that dominate the stratiform region are strongly influenced by the evolution of the leading convective region (e.g., Weisman 1992), we choose a reference frame for the stratiform domain that moves with the same speed and toward the same direction as the one used for the central convective domain.

The equations for the relative band-normal and band-parallel flow may be written as

$$u = (u_{er} - u_{\text{ref}})\,\sin\alpha + (v_{er} - v_{\text{ref}})\,\cos\alpha,$$

$$v = (v_{er} - v_{\text{ref}})\,\sin\alpha - (u_{er} - u_{\text{ref}})\,\cos\alpha,$$

where u_{er} and v_{er} are, respectively, the earth-relative zonal and meridional wind components; u_{ref} and v_{ref} are, respectively, the earth-relative zonal and meridional

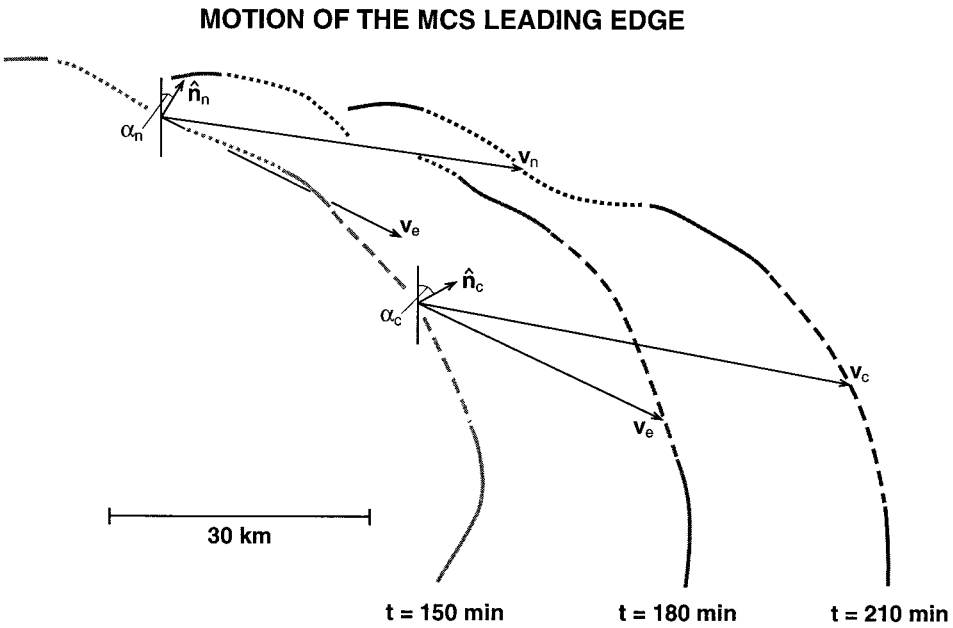

FIG. 5. Diagram indicating the respective earth-relative velocities $\mathbf{V}_n$ and $\mathbf{V}_c$ (long arrows) of the northern (dotted) and central (dashed) cold-pool edges from 150 to 210 min, and the relationship of these motions to both the respective local orientation vectors $\hat{\mathbf{n}}_n$ and $\hat{\mathbf{n}}_c$ (short arrows) of the northern and central cold-pool edges and the density-weighted mean environmental flow $\mathbf{V}_e$ (long arrow) determined from the initial hodograph of Fig. 1b. The angle α of the cold-pool orientation vector $\hat{\mathbf{n}}$ is measured clockwise from the north. The velocity vectors $\mathbf{V}_n$, $\mathbf{V}_c$, and $\mathbf{V}_e$ are scaled to represent distance traveled in the 1-h time increment at these constant velocities. The positions of the leading edge of the cold pool at 150, 180, and 210 min (indicated by the gray shading of variable intensity) are determined by the -0.01 m s^{-2} buoyancy contour at 500 m MSL, with buoyancy defined as in Eq. (1) of Trier et al. (1997).

components of the reference frame motion; and α is the angle measured clockwise from north that specifies the orientation of a vector directed normally outward from the local cold-pool edge. At 3 h, $u_{\text{ref}} = 10.4$ m s^{-1} and 12.1 m s^{-1}, $v_{\text{ref}} = -1.4$ m s^{-1} and -3.5 m s^{-1}, and $\alpha = 25°$ and 132° for the northern and southern convective domains, respectively. For the central convective and stratiform domains, $u_{\text{ref}} = 12.4$ m s^{-1}, $v_{\text{ref}} = -2.8$ m s^{-1}, and $\alpha = 70°$.

Figure 5 illustrates the motion of a portion of the leading edge of the cold pool. The precise locations of the northern (dotted) and central (dashed) cold-pool edges along the arc-shaped leading edge are determined in a manner that ensures continuity of the position of the northern mesoscale vortex (at 4 km MSL) relative to the location of these local cold-pool edges during the 1-h analysis period. For this period, the vortex circulation center remains along the northwestern boundary of the central convective domain, as depicted at 3 h (Fig. 4).

The northern and central cold-pool edges move in similar directions (toward 97.8° and 102.9°, respectively) despite their considerably different orientations (Fig. 5). In the central convective region, the angle between the local cold-pool orientation vector $\hat{\mathbf{n}}_c$ and the cold-pool motion vector $\mathbf{V}_c$ is relatively small, 33° (Fig. 5). The resulting substantial component of motion parallel to the leading-edge orientation vector is commonly observed in fast-moving convective bands. In contrast, the motion $\mathbf{V}_n$ of the northern cold-pool edge (73° to the right of $\hat{\mathbf{n}}_n$) is primarily perpendicular to the local cold-pool orientation vector $\hat{\mathbf{n}}_n$.

The motion of the cold pool is influenced by both translation due to the environmental flow in which the MCS is embedded and propagation due to the buoyancy (density) contrast across its leading edge. The small (3.1 m s^{-1}) component of the northern cold-pool edge motion ($|\mathbf{V}_n| = 10.5$ m s^{-1}) in the direction of its orientation vector $\hat{\mathbf{n}}_n$ is consistent with the local orientation vector being nearly perpendicular to the substantial (7.6 m s^{-1}) density-weighted mean environmental flow $\mathbf{V}_e$ (Fig. 5). Both the significantly smaller angle between the orientation vector of the central cold-pool edge $\hat{\mathbf{n}}_c$ and the environmental flow $\mathbf{V}_e$ (Fig. 5), and the particularly large buoyancy deficit of the central cold pool compared with other portions of the MCS (Trier et al. 1997, their Fig. 3a) favor the comparatively large (10.7 m s^{-1}) component of the central cold-pool edge motion ($|\mathbf{V}_c| = 12.7$ m s^{-1}) in the direction of its orientation vector. Internal circulations, such as the front-to-rear and rear-to-front flows associated with the counterrotating mesoscale vortices, may also locally influence cold pool motions (e.g., Weisman 1993; Skamarock et al. 1994).

In the forthcoming analysis, the vertical profiles of

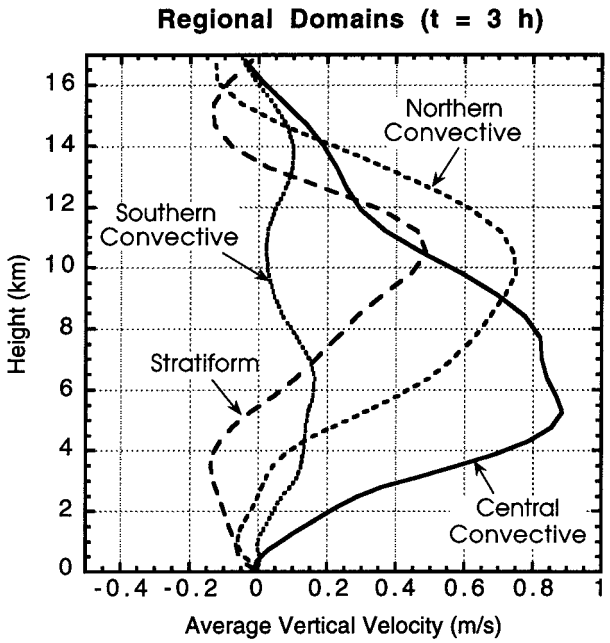

FIG. 6. Vertical profiles of horizontally averaged vertical velocity (m s^{-1}) within the 35 km × 30 km regional domains displayed in Fig. 3.

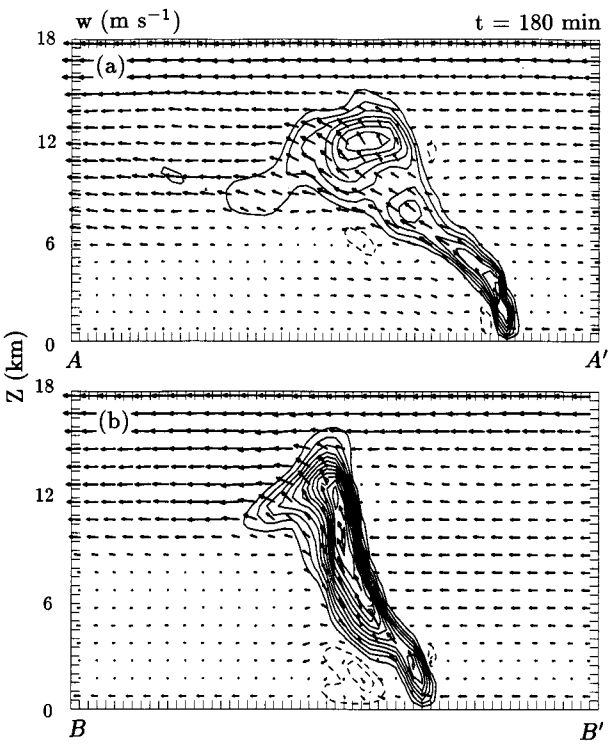

FIG. 7. System-relative flow vectors and the vertical velocity (1 m s^{-1} contour intervals; positive values solid, negative values dashed, zero contour eliminated) along transects (a) AA' and (b) BB' of Fig. 3. The vertical scale in both panels is exaggerated by a factor of 2.

the vertical motion and the vertical fluxes of the band-normal and band-parallel relative momentum (hereafter referred to as simply the band-normal or band-parallel momentum fluxes) are horizontally averaged. For each of these respective averaged quantities ($\overline{w}$, $\overline{\rho}\,\overline{uw}$, $\overline{\rho}\,\overline{vw}$) the averaging operator applied to a given quantity ( ) is defined by

$$\overline{(\,)} = \frac{1}{A}\int_A (\,)\, dA, \tag{1}$$

where the averages are taken over the area A of the individual sub-MCS-scale domains in Fig. 3.

b. Results

The averaged vertical velocity profiles from the four sub-MCS domains exhibit significant differences (Fig. 6). The central convective region has both the lowest (5 km MSL) and most intense (0.9 m s^{-1}) maximum areally averaged vertical motion. The amplitude and vertical structure of the central profile is similar to convective vertical motion profiles obtained in previous studies of tropical squall lines over averaging domains of similar size (e.g., Lafore et al. 1988). Unlike the profile from the central convective domain, the stratiform profile exhibits both a mean updraft and downdraft. The updraft peak is located substantially higher at 10.5 km MSL and is only half as strong as in the profile of the central convective domain. Johnson (1980), however, notes that despite the weakness of vertical motion profiles in stratiform regions, these motions are important to heat and moisture budgets since stratiform precipitation zones often cover substantial portions of tropical MCSs. The vertical profile of the northern convective region (Fig. 6) has a structure intermediate between the central convective and stratiform domains, with an elevated mean updraft peak at 10 km, and a weak mean downdraft located below 2.5 km. Areally averaged vertical motion over the southern convective domain, where convective updrafts are widely scattered, is considerably weaker than over the other three sub-MCS-scale domains.

Comparison of vertical cross sections taken through the central (Fig. 7a) and northern convective zones (Fig. 7b)[4] illustrates the narrower width and less substantial rearward updraft tilt of the northern convective zone in the middle and upper troposphere. The individual updraft cells are generally stronger at middle and upper levels in the northern convective region (Trier et al. 1997, their Fig. 6) despite the occurrence of the strong-

[4] The cross section through the northern convective zone is taken at an angle 25° from normal to the mean orientation of the leading edge. This is done to better illustrate the vertical structure of convection, since, unlike for the central region (where convective organization is locally quasi-two-dimensional), in the northern region convective cores are often oriented at a significant angle to the mean cross-line direction.

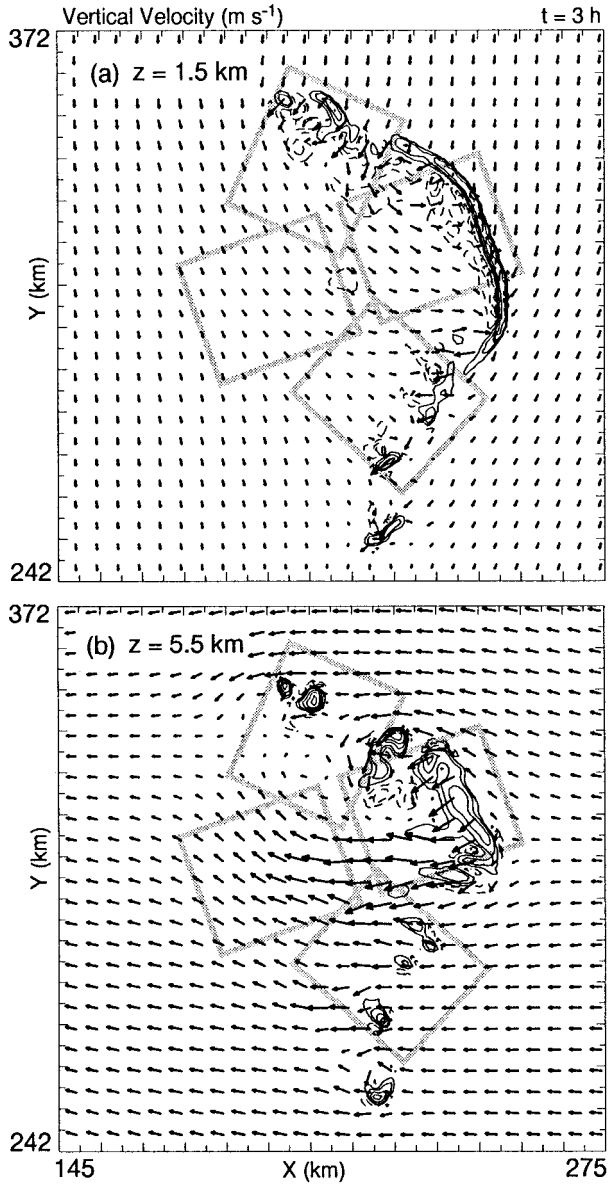

FIG. 8. Vertical velocity contoured at 1 and 2.5 m s^{-1} values, with additional positive values contoured in increments of 2.5 m s^{-1} (solid), and with negative values contoured at -0.5, -1.0, -1.5, and -2.0 m s^{-1} (dashed) for 3 h at (a) 1.5 and (b) 5.5 km MSL. System-relative horizontal flow vectors are plotted with a vector the length of the space between tick marks having a magnitude of 10 m s^{-1}. The rectangles represent the location of the regional domains as in Fig. 3.

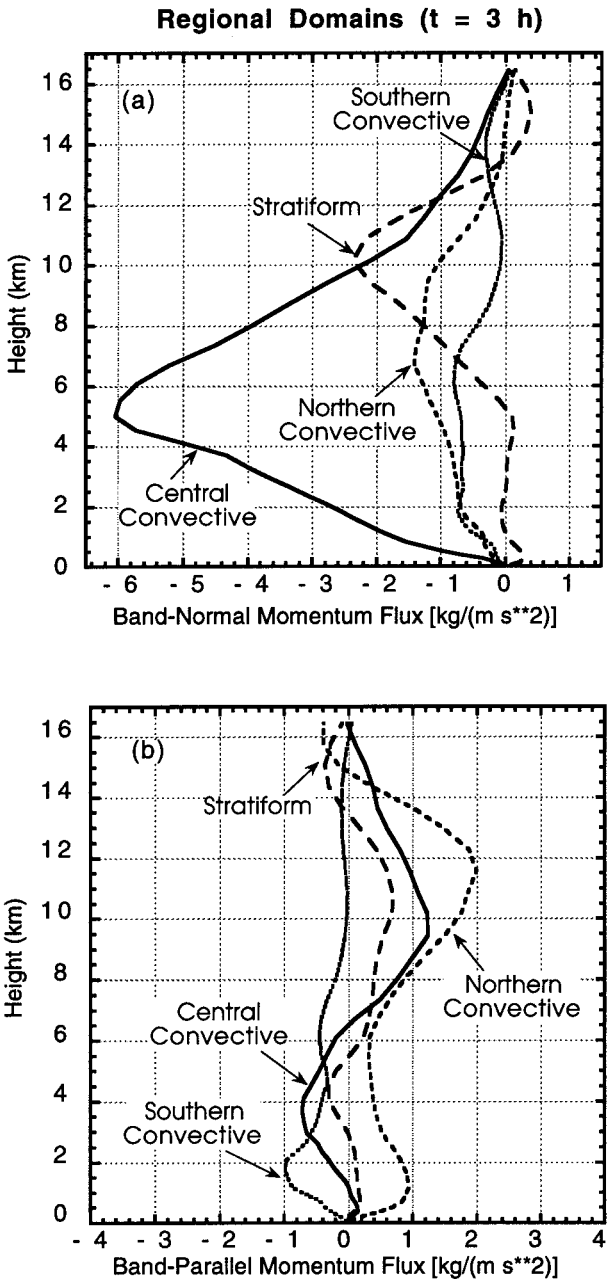

FIG. 9. Vertical profiles of the vertical flux of the relative horizontal momentum (kg m^{-1} s^{-2}) oriented (a) normal and (b) parallel to the leading-edge convective band at 3 h for the regional domains displayed in Fig. 3.

est areally averaged updraft at midlevels over the central convective domain (Fig. 6). The strong areally averaged vertical velocity at midlevels in the central convective region is explained by the greater coverage of the convective updraft zone in this portion of the MCS (Fig. 8).

The character and effect of the areally averaged momentum flux also differs substantially between the central and northern portions of the convective system, reflecting the different convective band orientations relative to the environmental vertical shear and the related differences in mesoconvective organization within these regions. Band-normal momentum fluxes (Fig. 9a) greatly exceed the band-parallel fluxes (Fig. 9b) in the central convective and stratiform domains, and are negative (directed rearward) through most of the troposphere, consistent with Doppler radar analysis of the observed MCS (Jorgensen et al. 1996, their Fig. 5).

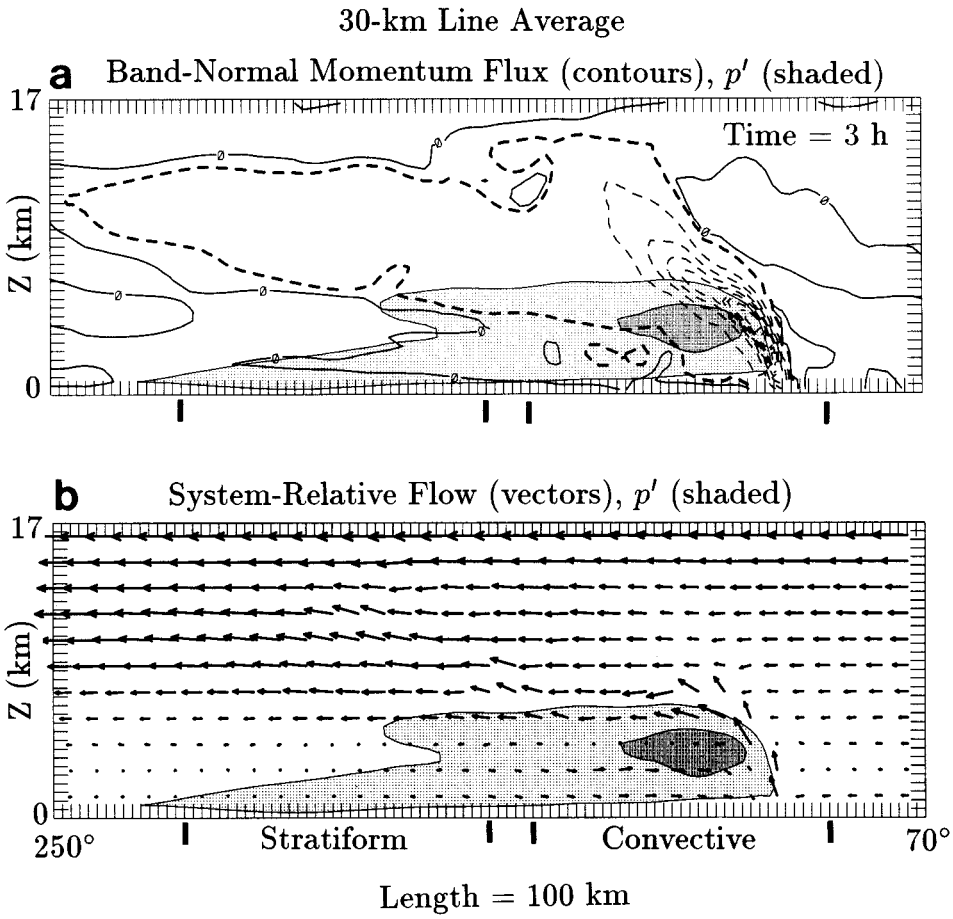

FIG. 10. The 30-km line-averaged vertical cross section at 180 min (3 h) that spans the central convective and stratiform regional domains displayed in Fig. 3. The pressure perturbation from initial conditions is shaded for values less than −0.1 (light) and −0.4 mb (dark). (a) Vertical flux of horizontal momentum oriented normal to the leading-edge convective band is contoured in intervals of 5 kg m^{-1} s^{-2} (thin lines; positive values solid; negative values dashed) with the bold contour enclosing regions of less than -5×10^{-1} kg m^{-1} s^{-2}. (b) System-relative flow in the plane of the cross section, with a vector the length of the space between tick marks having 2 m s^{-1} magnitude.

A line-averaged vertical cross section that extends through the central convective and stratiform domains (Fig. 10) exhibits the two-dimensional (cross-band) flow and momentum-flux features that occur nearly universally in observational and modeling studies of mesoscale convective bands. The negative momentum flux is locally strongest at midlevels in the rearward tilting convective updraft zone (Fig. 10a), where front-to-rear flow is accelerated rearward by the horizontal pressure gradient force (Fig. 10b), as found by LeMone (1983) for tropical convective bands in the Global Atmospheric Research Program's Atlantic Tropical Experiment (GATE) and by Smull and Houze (1987) for midlatitude squall lines. Although locally much weaker than in the leading convective zone, areally averaged rearward momentum flux is significant in the stratiform precipitation zone to the rear (cf. Figs. 9a and 10a), owing to strong front-to-rear flow and the mesoscale organization of the upper-tropospheric updraft.

In the central convective region a substantial component of the environmental shear at midlevels above the jet (Fig. 1b) is directed rearward, normal to the cold-pool edge (Fig. 3). This favors the development of a rearward tilting convective updraft zone (Fig. 7a) and subsequent development of a midlevel mesolow (Fig. 4), which arises in association with the vertical gradients of buoyancy[5] that result from the rearward updraft tilt. Once developed, the mesolow reinforces the strong band-normal accelerations. Along the north flank, where the midlevel shear (Fig. 1b) is directed parallel to the cold-pool edge (Fig. 3), the deep convective band remains more cellular (Fig. 8), does not develop as sub-

[5] As the MCS matures, local pressure minima are present in the vicinity of the vortices (Fig. 4). In addition to the contribution to low pressure from buoyancy, smaller-scale dynamical lowering of the pressure, which is associated with rotation (e.g., Klemp and Rotunno 1983; Brandes 1984), contributes significantly to the pressure field in the vicinity of these minima (Trier et al. 1997, their Fig. 4).

stantial a rearward tilt (Fig. 7b), and thus lacks the mid-level mesolow (Fig. 4) and strong front-to-rear flow (Fig. 8b) present in the central convective region. Hence, although of the same rearward sense, the band-normal momentum flux in the northern convective region is considerably weaker than in the central convective zone (Fig. 9a).

The alignment of the north flank precipitation band, parallel to the middle- and upper-tropospheric vertical shear, promotes band-parallel momentum flux. Here, the band-parallel momentum flux greatly exceeds that of the band-normal momentum flux in the upper troposphere (Fig. 9) and, by being maximized in the upper troposphere (Fig. 9b), supports along-band accelerations (toward ESE) in the middle troposphere. Significant momentum-flux forcing for accelerations along convective bands is common in observations (e.g., LeMone and Moncrieff 1994) and numerical simulations (e.g., Dudhia and Moncrieff 1987) of slow-moving convective bands that are parallel to the middle- and upper-tropospheric vertical shear. In the northern convective domain, the momentum-flux forcing acts to reduce the magnitude of the band-parallel flow, which contrasts with the predominantly band-normal momentum-flux forcing in the central convective and stratiform domains that acts to enhance the magnitude of the band-normal flow (above the level of maximum rearward momentum flux, Fig. 9a).

5. MCS-scale accelerations

We now examine horizontal accelerations averaged over the 200 km $\times$ 200 km domain (hereafter referred to as the ''large-scale'' or ''MCS-scale'' domain) depicted earlier in Fig. 2, which covers the precipitation area associated with the MCS and represents a typical horizontal resolution used in current GCMs. We focus on horizontal accelerations over the period from 3 to 5 h, during which the MCS attains the asymmetric three-dimensional structure displayed in Fig. 2b. It is important to realize, however, that changes in the intensity and vertical structure of the MCS-scale accelerations occur during the simulation. Moreover, the intensity and vertical structure of the horizontal accelerations will also vary with environmental conditions. Thus, the details of the vertical profiles of horizontal accelerations presented in the forthcoming analysis should not be interpreted as a general statement of how this type of MCS influences the large-scale flow. Instead, our purpose is to illustrate how the three-dimensionality and associated spatial variability in mesoconvective structure, shown in the previous section, can influence MCS-scale accelerations. Since three-dimensional structure associated with line-end effects is present to some extent in most squall-type MCSs, the forthcoming results are likely relevant to a sizeable portion of the spectrum of MCS organization.

a. Zonal and meridional accelerations

In our analysis of sub-MCS-scale variability, we examined the horizontal flow and momentum fluxes in a coordinate system that had its axes oriented parallel and perpendicular to the local orientation of the MCS leading edge. While we can define a mean orientation of the arc-shaped leading edge, it is most straightforward to analyze the flow on the MCS scale in terms of its zonal and meridional components. Thus, in this section and in the following section (where a momentum budget is calculated) u and v, respectively, represent the *zonal* and *meridional* wind components relative to the constant model domain speed of 10.6 m s^{-1} toward 101°, which is an approximate mean motion of the leading edge of the MCS. While there is a $\sim$0.5 m s^{-1} h^{-1} acceleration of the leading edge during the 2-h analysis interval, performing the calculations of the horizontal accelerations within a reference frame that translates at constant speed simplifies interpretation since, in such a reference frame, accelerations are invariant.

Over the large-scale domain, the average relative zonal and meridional wind components do not change by more than 0.75 m s^{-1} during the 2-h period (Fig. 11a). The strongest accelerations are present in the zonal component over the lowest 1 km. A second layer of enhanced eastward acceleration occurs in the upper troposphere between 9 and 14 km, but does not reach the strength of the near-surface accelerations (Fig. 11a).

The strength of the horizontal accelerations associated with the simulated MCS are nearly an order of magnitude smaller than those of a quasi-two-dimensional midlatitude squall line analyzed using rawinsonde data (Gallus and Johnson 1992) and output from a two-dimensional cloud-resolving model (Yang and Houze 1996) over a comparable horizontal scale. These differences likely result from a combination of factors including the relatively weak convective and mesoscale circulations of this tropical MCS compared to the midlatitude case, the likelihood that the larger midlatitude MCS significantly perturbs the flow over a greater percentage of the domain in which areal averages are calculated, and effects of three-dimensionality (described in the next subsection) that are sampled in the current tropical case.

Because of the typically weak large-scale (environmental) advections and pressure gradients in the Tropics, the relatively weak horizontal accelerations induced by the MCS are still potentially important. The zonal accelerations in the lowest levels are particularly noteworthy since they result in increased ground relative winds just above the ocean surface and, hence, enhanced air–sea fluxes commonly observed with oceanic squall-type precipitation systems (Young et al. 1995; Weller and Anderson 1996). The low-level accelerations produced by individual squalls or groups of this type of precipitation system may also reinforce the low-level westerlies associated with synoptic-

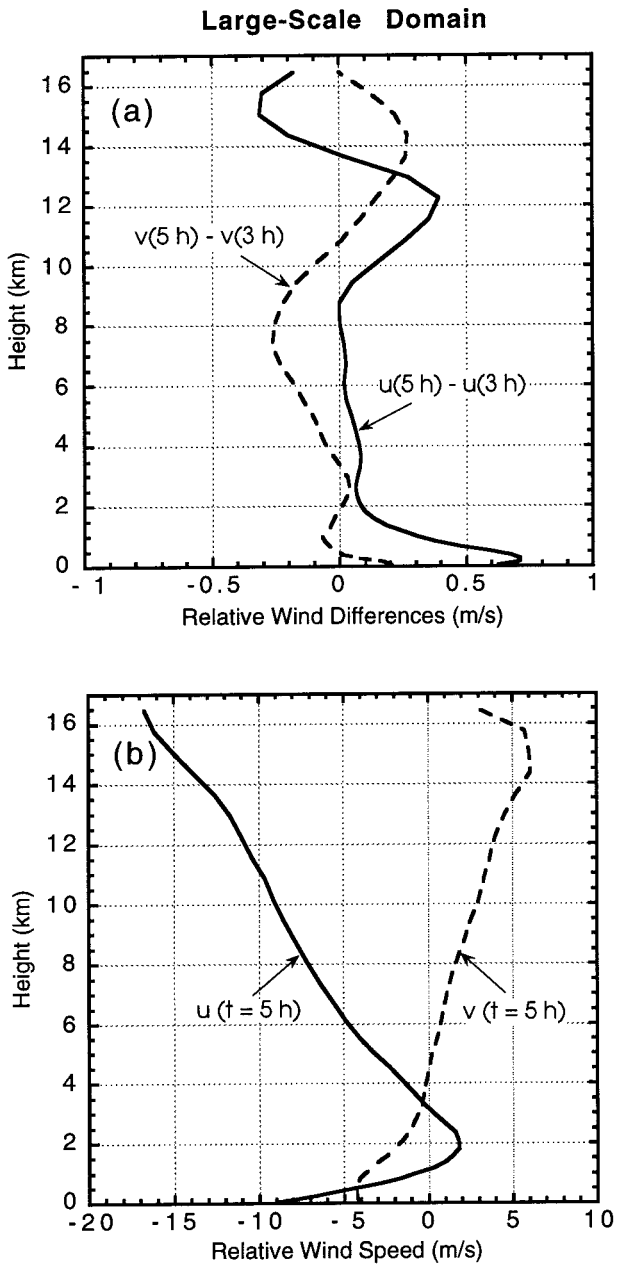

FIG. 11. (a) Vertical profiles of the 2-h tendency of the horizontally averaged zonal (solid) and meridional (dashed) relative momentum between 3 and 5 h, and (b) vertical profiles of the zonal (solid) and meridional (dashed) relative momentum at 5 h for the large-scale domain shown in Fig. 2.

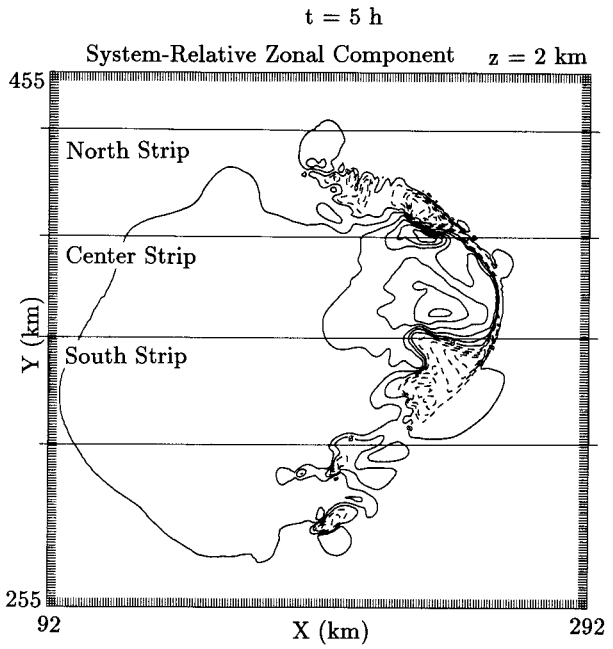

FIG. 12. The 2-km MSL relative zonal momentum at 5 h over the 200 km × 200 km large-scale domain of Fig. 2 contoured in intervals of 2 m s^{-1}. The 200 km × 40 km strips signify the north, center, and southern subdomains over which separate contributions to the averages presented in Fig. 13 are computed. Positive values are solid; negative values are dashed.

scale westerly wind bursts[6] that occur during the tropical intraseasonal oscillation (Madden and Julian 1972, 1994).

Comparison of the zonal wind changes (Fig. 11a) with the zonal wind profile (Fig. 11b) indicates that, on the large scale, the MCS influences the zonal vertical shear differently in four distinct layers. The 2-h tendency is to reduce the eastward shear beneath the low-level jet, to very weakly increase the midlevel westward shear above the jet, to reduce westward shear in the layer from 9 to 12 km, and to increase the westward shear from 12 to 15 km. The primary effect of the meridional accelerations during the period from 3 to 5 h is to weaken the midlevel northward shear from 3 to 8 km, while strengthening the northward shear from 8 to 14 km (Figs. 11a and 11b).

b. Impact of three-dimensionality on MCS-scale accelerations

The analyses over MCS subdomains presented in section 4 illustrate the three-dimensionality and associated systematic spatial variability of mesoconvective structure that can occur within MCSs. Quantitative comparisons of the wind tendencies within these smaller domains with those of the large-scale domain are complicated by several factors, including the differences in the specification of coordinate systems (e.g., relative to earth geometry in the MCS-scale analysis, while relative to local MCS orientation in the sub-MCS-scale analysis), and are not attempted. However, insight into how three-dimensionality influences the vertical profile of horizontal accelerations on the MCS scale may be gained by subdividing a portion of the current large-scale domain into three 200 km × 40 km strips (Fig. 12), and

[6] The onset of westerly wind bursts over the equatorial western Pacific are commonly associated with widespread deep convection (e.g., Kiladis et al. 1994; Lin and Johnson 1996; Chen et al. 1996).

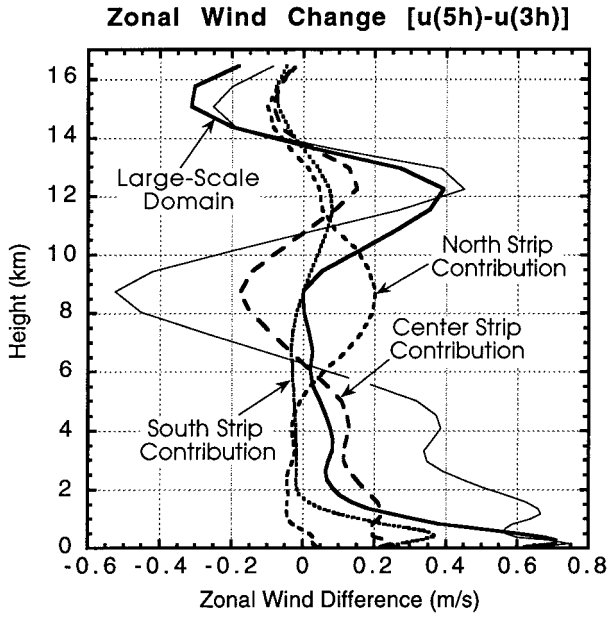

FIG. 13. Vertical profiles of the 2-h tendency (differences) of horizontally averaged relative zonal momentum (m s^{-1}) between 3 and 5 h over the 200 km × 200 km domain displayed in Figs. 2 and 12 (bold solid) and the contributions to this MCS-scale difference (see text) from the north (medium dash), south (small dash), and center (large dash) 200 km × 40 km^2 subdomains displayed in Fig. 12. The thin solid curve represents the contribution from the center strip multiplied by a factor of 3. This curve can be compared to the bold solid line to ascertain the representativeness of the zonal accelerations in the center strip for the purpose of estimating those of the entire MCS (see text for explanation).

examining the horizontally averaged wind tendencies within these strips.

The north strip surrounds the expanding north flank rainband (cf. Figs. 12 and 2b). The center strip encompasses both the rear-inflow zone and the enhanced front-to-rear flow located above, which are associated with the bow-shaped precipitation feature and the midlevel transverse precipitation band located to the rear at its southern edge (cf. Figs. 12 and 2b). The character of the convection and mesoscale flow within the center strip is similar to that of the area composed of the central convective and stratiform sub-MCS-scale domains discussed in the previous section. The south strip contains shallow updraft cells within enhanced low-to-midlevel front-to-rear flow south of the bow (cf. Figs. 12 and 2b).

The areally averaged zonal-wind changes from 3 to 5 h for the large-scale domain and its individual contributions from the north, center, and south strips are displayed in Fig. 13. The contribution from an individual strip is given by $\Delta u_s = u_s(5\text{ h}) - u_s(3\text{ h})$, where

$$u_s = \frac{A_s}{A_{ls}}\overline{u_s}, \tag{2}$$

with

$$\overline{u_s} = \frac{1}{A_s}\int_{A_s} u\, dA$$

representing the average of the system-relative zonal wind u over the area A_s of the strip. The coefficient $A_s/A_{ls} = 0.2$, which multiplies $\overline{u_s}$ in (2), results from a normalization that accounts for the five-fold greater area of the large-scale domain A_{ls} than that of the individual strips A_s. However, since the three individual strips are situated over the most disturbed region of the large-scale domain (Fig. 12), it is not surprising that their net contribution accounts for nearly the entire zonal-wind tendency over the large-scale domain (Fig. 13).

The leading edge of deep convection within the center strip is oriented north–south, within ~10° of being normal to the environmental vertical shear in the lowest 2 km (cf. Figs. 1b and 12). Hence, in a local sense, the zonal accelerations within this strip represent band-normal front-to-rear and rear-to-front accelerations that are nearly aligned with the low-level vertical shear. MCS orientation nearly normal to the environmental low-level vertical shear is characteristic of fast-moving tropical convective bands (Barnes and Sieckman 1984; Alexander and Young 1992; LeMone et al. 1998). Thus, it is not surprising that vertical structure of the zonal accelerations in this portion of the MCS closely resembles the vertical structure of band-normal accelerations found in radar observations of portions of squall-type convective bands (e.g., Smull and Houze 1987; Lin et al. 1990) and in two-dimensional numerical simulations of squall lines (e.g., Yang and Houze 1996). These accelerations include an increase in the rear-to-front (eastward) flow through the lowest 6 km, an increase in the front-to-rear (westward) flow in the 6–11-km layer, and an increase in the rear-to-front (eastward) flow aloft from 11 to 14 km (Fig. 13).

Extrapolation of the effects of convection on the environmental flow near the center of the MCS to the more peripheral north and south strips would, however, lead to significant errors in the MCS-scale horizontal accelerations and an overestimation of the magnitude of the zonal vertical shear increases through a substantial portion of the midtroposphere. The thin solid line in Fig. 13 indicates the MCS-scale zonal acceleration that would result if the zonal accelerations in the north and south strips were identical to those in the center strip. For instance, making the assumption that the accelerations within the center strip are representative of those of the entire MCS implies an increase in the magnitude of the zonal vertical shear between 2 and 9 km MSL of 1 m s^{-1},[7] whereas the actual increase (bold solid line)

[7] This estimate is constructed by multiplying the contribution to the MCS-scale acceleration from the center strip by a factor of 3 (instead of 5) since the area outside of the three strips, which represents two-fifths of the area of the large-scale domain, contributes a relatively small amount to the areally averaged acceleration.

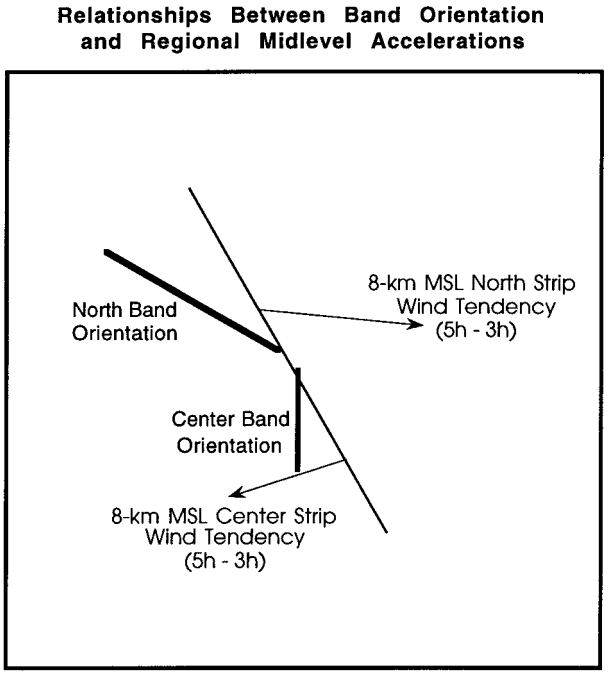

FIG. 14. Schematic diagram of the relationship between convective band orientation (bold solid lines) and the 8-km MSL regional accelerations from 3 to 5 h (thin arrows) in the 200 km × 40 km north and center strips displayed in Fig. 12.

in the large-scale domain is only 0.1 m s^{-1}. Only in the lowest 500 m and in the upper troposphere above 12 km are the accelerations in the center strip representative of those of the entire MCS (Fig. 13). The relatively weak MCS-scale zonal accelerations through much of the lower and middle troposphere result from cancellation among the center strip and the north and south strips.

The relationship between the midtropospheric horizontal accelerations and the orientation of the leading convective bands in the north and center strips, where these accelerations most strongly oppose each other (Fig. 13), is illustrated schematically in Fig. 14. From this diagram, it is evident that the differences in midlevel accelerations within these strips result from differences in both the orientation of the bands relative to the strips (three-dimensionality) and the different character of accelerations relative to band orientation within the individual strips. For the center portion of the MCS, the midlevel accelerations are primarily normal to the leading convective band and result in increased midlevel vertical shear in the direction opposite to system motion, much as is found in conceptual models of squall lines (e.g., Moncrieff 1992). In contrast, the midlevel accelerations in the northern strip are directed primarily parallel to the leading convective band, and result in strong cancellation with the primarily zonal, but oppositely directed accelerations within the center strip (Fig. 14).

The differences in accelerations between the north and center strips are consistent with the contrasting character and effect of the momentum flux on midlevel accelerations in the northern and central convective regions discussed earlier in section 4b, which themselves are a consequence of differences in mesoconvective organization arising from the different orientations of the precipitation bands relative to the environmental vertical shear. Because of the strong cancellations of the zonal acceleration component among the strips (Fig. 13), midtropospheric accelerations on the MCS scale are primarily in the meridional direction (Fig. 11a), which is nearly normal to both the direction of mean MCS motion and the low-level vertical shear (Fig. 1b).

6. MCS-scale momentum budget

We have demonstrated that the large-scale accelerations during the three-dimensional asymmetric stage of the precipitation system differ substantially from those over distinct subregions. In this section we examine the forcing of these mean horizontal accelerations over the large-scale domain. To do so, we use the horizontally averaged momentum equations obtained by combining the flux form of the horizontal momentum equations with the anelastic continuity equation ($\nabla \cdot \overline{\rho}\mathbf{v} = 0$), and then applying the horizontal averaging operator (1), where, in this case, A refers to the area of the large-scale domain A_{ls}. In the resulting equations

$$\frac{\partial \overline{u}}{\partial t} = \underbrace{-\frac{1}{\overline{\rho}}\frac{\partial \overline{p}}{\partial x}}_{u\text{-PGF}} \underbrace{-\frac{1}{\overline{\rho}}\frac{\partial}{\partial z}(\overline{\rho}\,\overline{uw})}_{u\text{-VTR}} \underbrace{-\overline{\nabla_H \cdot u\mathbf{v}_H}}_{u\text{-HTR}}, \quad (3)$$

$$\frac{\partial \overline{v}}{\partial t} = \underbrace{-\frac{1}{\overline{\rho}}\frac{\partial \overline{p}}{\partial y}}_{v\text{-PGF}} \underbrace{-\frac{1}{\overline{\rho}}\frac{\partial}{\partial z}(\overline{\rho}\,\overline{vw})}_{v\text{-VTR}} \underbrace{-\overline{\nabla_H \cdot v\mathbf{v}_H}}_{v\text{-HTR}}, \quad (4)$$

the domain-averaged accelerations $\overline{u_t}$, and $\overline{v_t}$ are, respectively, for the system-relative zonal and meridional wind components. The three terms on the right side of these equations represent the forcing of accelerations associated with the mean horizontal pressure gradient (PGF), the vertical convergence of the vertical momentum flux (vertical transport; VTR), and the horizontal convergence of the horizontal momentum flux (horizontal transport; HTR).

Using the definition of the horizontal averaging operator (1) and applying the two-dimensional divergence theorem, the horizontal transport terms from (3) and (4) may alternatively be written as

$$-\overline{\nabla_H \cdot u\mathbf{v}_H} = -\frac{1}{A_{ls}}\oint u\mathbf{v}_H \cdot \mathbf{n}\, dl,$$

$$-\overline{\nabla_H \cdot v\mathbf{v}_H} = -\frac{1}{A_{ls}}\oint v\mathbf{v}_H \cdot \mathbf{n}\, dl,$$

where **n** is a unit vector directed locally outward from the domain boundary, and *dl* is an infinitesimal length along the boundary. In this representation, only the fluxes of the horizontal momentum components through the boundaries of the domain (averaged along its perimeter) contribute to the horizontal transport term.

The forcing terms in (3) and (4) are calculated over the large-scale domain at 3, 4, and 5 h and then averaged. As a check on the reliability of the time-averaged forcing, the tendency predicted from the forcing is compared to the actual tendency calculated from the domain-averaged wind components at 3 and 5 h.

The zonal forcing has a vertical structure that is quite similar to that of the zonal tendency (Fig. 15a). The zonal accelerations derived from the forcing terms are generally within 0.05 m s^{-1} h^{-1} of the actual accelerations. Some discrepancy between the two profiles occurs at the lowest levels where the forcing overpredicts the actual zonal acceleration, and in a portion of the midlevels, where small-amplitude structure in the forcing is not apparent in the actual tendency profile.[8] Similarly, the time-averaged meridional accelerations derived from the forcing closely resemble the actual meridional accelerations (Fig. 15b).

The contribution of the forcing terms in (3) and (4) to the respective zonal and meridional accelerations are presented in Fig. 16. Due to substantial cancellation among the forcing terms (Fig. 16), the accelerations (Fig. 15) are generally much weaker than the individual components of the forcing. This result is consistent with previous momentum budget studies over a wide range of scales. The horizontal transport term is roughly 180° out of phase with the vertical transport term and the sum of these two terms is partly compensated for by the horizontal pressure gradient force. Lafore et al. (1988) found a similar relationship on smaller scales between the forcing terms from radar observations and simulations of a west African squall line.

As noted in the previous section, the strongest relative accelerations are associated with the near-surface and upper-tropospheric zonal component. These eastward accelerations are dominated by the vertical and horizontal transport terms, respectively (Fig. 16a). The effect of the horizontal transport term on the eastward acceleration aloft can be understood by examining the upper-level flow at 12 km within the large-scale domain (Fig. 17a). Here, there is a greater flux of westward ($u < 0$) momentum by northward ($v > 0$) flow out the northern boundary of the domain than through the southern boundary into the domain, as well as a stronger flux of westward momentum by westward flow out the western boundary of the domain than into the eastern boundary. These horizontal fluxes result in a net loss of westward momentum and hence an eastward domain-averaged acceleration (Fig. 16a). There is also a greater flux of northward momentum by the northward flow

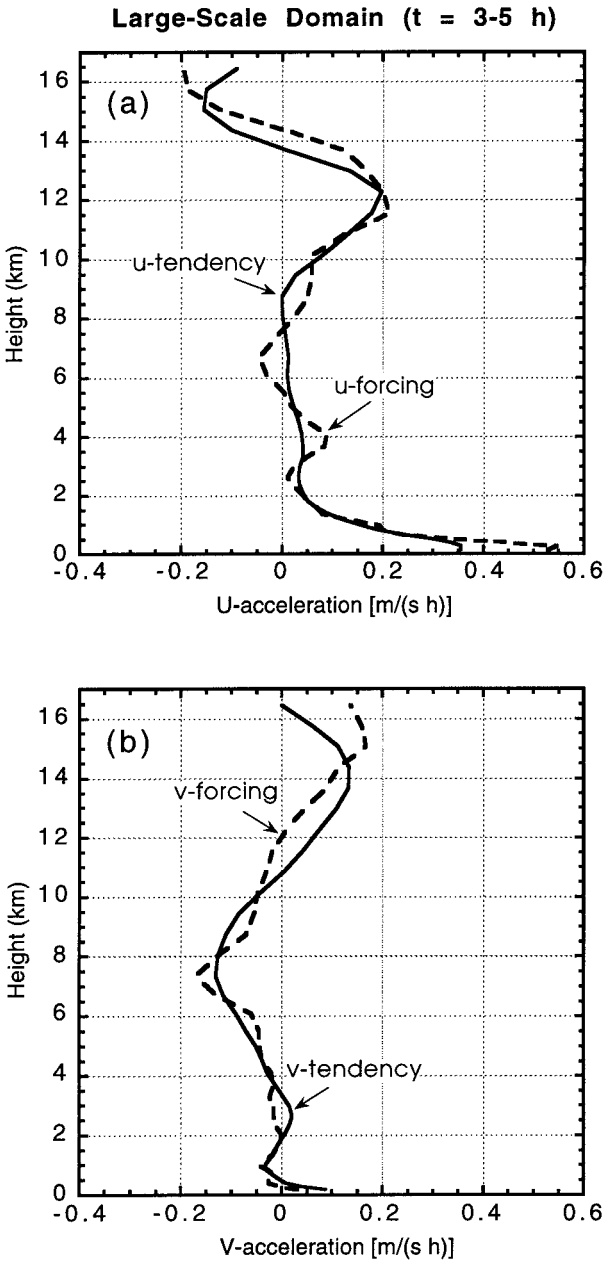

FIG. 15. Vertical profiles of the simulated 2-h tendencies (m s^{-1} h^{-1}) from 3 to 5 h (solid) and the time-averaged accelerations for the identical 2-h period that result from the forcing terms in Eqs. (3) and (4) (dashed) for the relative (a) zonal and (b) meridional momentum horizontally averaged over the 200 km × 200 km domain displayed in Figs. 2 and 12.

[8] Small differences between the 2-h wind change tendencies and the tendencies derived from the time-averaged forcing result, in part, from the exclusion of both physical and computational mixing in the horizontal momentum equations. Moreover, direct comparisons between the tendencies and forcing are complicated by the fact that the 2-h wind change tendencies represent integrated evolution over a finite time interval, whereas the forcings for the tendencies constitute an average of instantaneous values at three times, and are thus expected to be more sensitive to high-frequency variations.

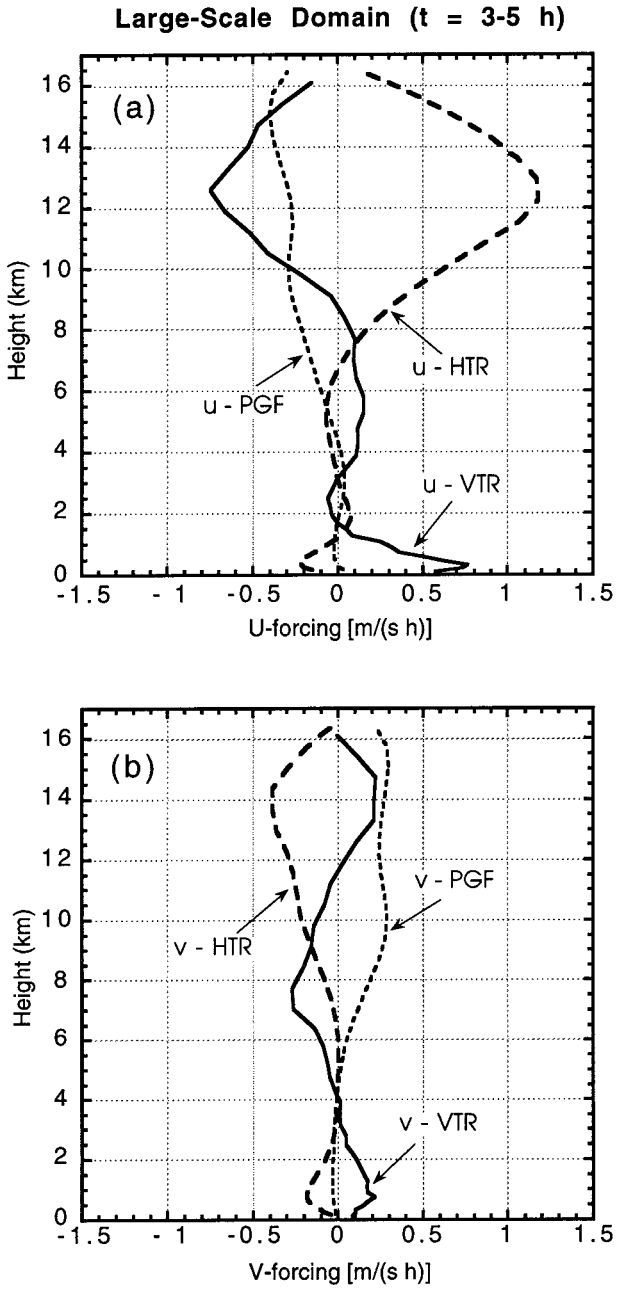

FIG. 16. Vertical profiles of the time-averaged (from 3 to 5 h) relative (a) zonal and (b) meridional accelerations (m s^{-1} h^{-1}) resulting from the individual forcing terms on the right side of Eqs. (3) and (4), respectively, horizontally averaged over the 200 km × 200 km domain displayed in Figs. 2 and 12.

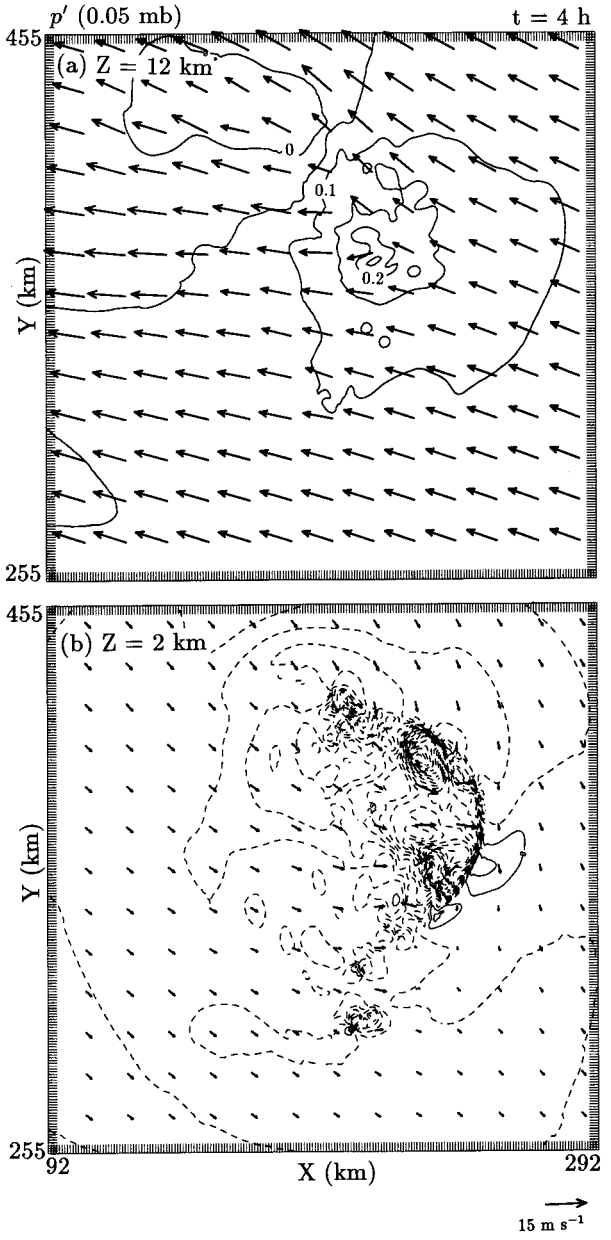

FIG. 17. Pressure perturbation from ambient conditions (0.05-mb contour interval) and approximate system-relative winds at 4 h for (a) 12 km MSL and (b) 2 km MSL. Positive values are solid; negative values are dashed.

through the northern boundary than into the southern boundary of the domain (Fig. 17a) that largely accounts for the forcing of southward acceleration by the horizontal transport term (Fig. 16b). In contrast, at 12 km the vertical flux convergence and the meridional pressure gradient force compensate the effects of the horizontal transport (Figs. 16b) on the meridional wind component and less meridional than zonal acceleration results.

The acceleration of the flow toward the northwest over the northern part of the domain is accomplished by a broad, but relatively weak horizontal pressure gradient that extends beyond the midlevel precipitating region (cf. Figs. 2b and 17a) asymmetrically in the direction of the upper-level vertical shear (Fig. 1b). Locally, the maximum upper-level pressure gradient force is nearly an order of magnitude weaker than that as-

sociated with the low-to-midlevel mesolow (Fig. 17b). However, its influence on domain-averaged horizontal accelerations is greater than at low levels (Fig. 16). This is because while the low-to-midlevel mesolow contributes to strong localized accelerations in both the convective and stratiform regions (Fig. 4), its horizontal extent is too small to directly produce significant zonal or meridional domain-averaged accelerations beneath 5 km MSL through the pressure gradient terms in (3) and (4). Nevertheless, the potential indirect importance of the mesolow and also the surface mesohigh to the large-scale (domain-averaged) accelerations at lower and midlevels should not be dismissed, since these pressure features are significant sources of momentum generation on smaller scales that may contribute to the large-scale accelerations through the vertical transport terms in (3) and (4).

Large MCSs typically affect the upper-tropospheric pressure and flow fields over substantial distances (e.g., Fritsch and Maddox 1981). In the current case, the 200 km $\times$ 200 km domain encompasses the entire area of precipitation associated with the simulated MCS (Fig. 2), although the upper-level pressure and flow fields exhibit perturbations from initial conditions extending beyond its northern and western boundaries with magnitudes of up to $\sim$0.05 mb and several meters per second, respectively. If the domain is enlarged to completely enclose pressure and horizontal flow gradients, the pressure gradient (PGF) and horizontal flux convergence (HTR) terms in (3) and (4) will vanish. However, the vertical flux convergence (VTR) terms (which do not involve horizontal derivatives), while being reduced in magnitude, should basically retain their vertical structure. In this sense, the character of the vertical flux convergence is less dependent on the size of the domain, provided that the entire region of significant vertical motion is sampled, which is the case in the current analysis.

In a manner similar to the MCS-scale zonal accelerations presented earlier in Fig. 13, we divide the portion of the zonal acceleration that results from the vertical flux convergence into contributions from the individual 200 km $\times$ 40 km strips (Fig. 18). While the vertical patterns of these accelerations are different from the total zonal accelerations (Fig. 13), there are, again, significant differences between the center strip and the north and south strips. The differences are particularly striking in the middle troposphere and portions of the upper troposphere. From 4 to 10 km, most of the MCS-scale vertical flux convergence of the zonal component comes from the center strip. Thus, extrapolation of the vertical flux convergence in the center strip to the end regions of the MCS contained in the north and south strips would, as with the total accelerations (Fig. 13), lead to MCS-scale overprediction of both the eastward acceleration from this effect and the resulting increases in the magnitude of zonal vertical shear from 8 to 12 km at the top of this layer (Fig. 18).

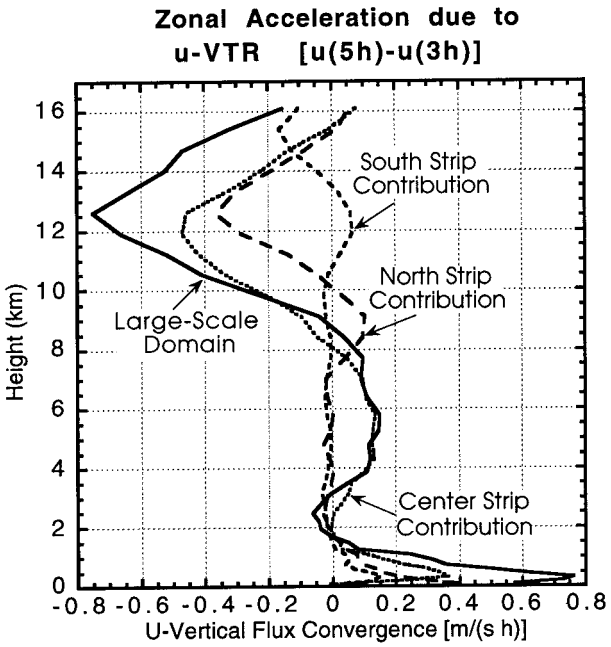

FIG. 18. Vertical profiles of the contribution of the horizontally averaged tendency of relative zonal momentum (m s^{-1} h^{-1}) from the vertical flux convergence term (*u*-VTR) in Eq. (3) averaged from 3 to 5 h over the 200 km $\times$ 200 km MCS-scale domain displayed in Figs. 2 and 12 (solid) and the contribution to this MCS-scale average from the north (large dash), south (medium dash), and center (small dash) 200 km $\times$ 40 km subdomains displayed in Fig. 12.

7. Summary and discussion

a. Summary

In this study we have examined the 200 km $\times$ 200 km scale (stormwide) horizontal accelerations associated with a simulated squall-type MCS. Our focus is on accelerations during the period when the MCS exhibits pronounced three-dimensional structure. Areally averaged momentum fluxes and horizontal accelerations over various subregions of the MCS are also presented, both to facilitate comparison with past Doppler radar and numerical studies over domains that are smaller than MCS scale, and to better understand the role of three-dimensionality and the related spatial variability of mesoconvective structure on the larger-scale modification of the horizontal flow. We find that while the sub-MCS-scale effects of deep convection on the horizontal flow are similar to those found in previous studies, the system-scale three-dimensional structure precludes determination of how the MCS modifies the flow on larger scales simply from analyzing momentum effects over any given sub-MCS-scale region.

The strongest MCS-scale accelerations occur near the surface and lead to stronger ground-relative winds, which promote enhanced air–sea fluxes. The zonal accelerations are considerably stronger than the meridional accelerations in both the lower (beneath 2 km MSL) and portions of the upper (10–12 km MSL) troposphere

and are directed eastward, which is nearly parallel to the mean MCS leading-edge motion vector (101°), and the environmental shear vector (80°) beneath the low-level jet. A momentum budget calculated over the identical 200 km × 200 km area reveals that the low-level accelerations are dominated by the vertical flux convergence term, whereas the upper-tropospheric accelerations are dominated by the horizontal flux convergence term. Zonal MCS-scale accelerations within the middle troposphere (2–9 km MSL) are weaker than the meridional accelerations, owing to substantial cancellation of accelerations among different portions of the MCS.

b. Implications

Past work has distinguished mesoscale convective bands, including both slowly moving linear bands and fast-moving squall lines that may contain extensive stratiform precipitation regions, from other forms of deep convection. The distinction is that the band-normal horizontal accelerations associated with these linear systems (rear-to-front at low levels, and front-to-rear through the middle troposphere) tend to increase the vertical shear through a deep tropospheric layer in the direction opposite to MCS propagation. This result has formed the basis for efforts to develop two-dimensional dynamically based schemes (e.g., Moncrieff 1992) to parameterize the effect of mesoscale deep convection on the horizontal flow in large-scale models.

Two-dimensional models determine momentum effects based on a priori specification of the environmental flow normal to the orientation of the MCS, which is also constrained by the two-dimensional framework to be in the same plane as system propagation. While the strength of the line-normal vertical shear is an important factor in how the convective band locally modifies the flow, a limitation of two-dimensional models is their inability to satisfactorily represent more realistic three-dimensional MCS structure in environments that possess directional vertical shear.

In the current case, the flow structure has characteristics of squall-type convection over a sizeable zone within the central portion of the MCS, which is oriented normal to the low-level vertical shear. These characteristics include the jump-updraft inflow branch and the rear-to-front overturning downdraft idealized by Moncrieff (1992). Over this region, strong horizontal accelerations resemble those from studies using two-dimensional numerical models (e.g., Yang and Houze 1996) and similarly result in substantial increases in the magnitude of the midtropospheric vertical shear in the direction opposite to MCS propagation. However, on the scale of the entire MCS, the vertical structure of the accelerations in the direction of the environmental low-level vertical shear is quite different from that of the central portion, and does not promote such strong increases in the magnitude of the midtropospheric vertical shear as would be expected if the entire system influenced the large-scale flow in a manner similar to the central region. The difficulty in determining the large-scale effect of deep convection on the vertical shear, based on examination of limited portions of the MCS, results from the three-dimensional structure of the MCS leading edge and its relationship to the environmental shear profile, in which the direction of the vertical shear varies with height (cf. Fig. 1b and 2b). The latter aspect promotes strong differences in mesoconvective structure within the MCS and associated differences in the strength and character of the horizontal accelerations in different regions.

Pronounced systematic variability in mesoconvective structure can also occur in simpler unidirectional environmental vertical shear when Coriolis accelerations modulate line-end circulations (e.g., Davis and Weisman 1994; Skamarock et al. 1994). Moreover, climatological studies (e.g., Loehrer and Johnson 1995) have indicated that squall-type MCSs spend a significant portion of their life cycle as three-dimensional precipitation systems. Hence, such three-dimensional organization may need to be considered in order to predict effects of these MCSs, integrated over their life cycle, on the larger-scale flow.

The use of two-dimensional schemes to parameterize the effects of organized convection in large-scale models may thus be best suited for certain subsets of mesoscale convection. For example, LeMone et al. (1998) found that slower-moving TOGA COARE mesoscale convective bands that were oriented parallel to midtropospheric (800–400 mb) vertical shear maintained a two-dimensional structure. For fast-moving squall-type systems that tend to occur in environments of stronger low-level shear, use of two-dimensional schemes may be more appropriate for systems of greater length than the one analyzed in the current study. The overall structure of such systems would conceivably be less influenced by line-end effects and would thus remain more linear (i.e., two-dimensional). Fully three-dimensional numerical models have, however, experienced difficulty in producing such linear squall-type MCSs in the absence of persistent external linear forcing (e.g., Tao and Simpson 1989; Skamarock et al. 1994). In midlatitudes, such forcing could be associated with surface cold fronts or upper-level baroclinic disturbances. However, in the Tropics the larger-scale forcing is more subtle and less well understood. In such environments, self-organization of mesoscale deep convection may be comparatively more important.

Acknowledgments. This work began as a portion of the first author's Ph.D. dissertation research in atmospheric science at Colorado State University (CSU). Richard Johnson, the first author's adviser at CSU, is thanked for his constructive comments and encouragement of this research. Comments on the manuscript from two anonymous reviewers and those from earlier inter-

nal reviews by Scott Braun (NCAR) and Christopher Davis (NCAR) improved the presentation of this work. Portions of this research were supported by the National Science Foundation (Grant 9215507).

REFERENCES

Alexander, G. D., and G. S. Young, 1992: The relationship between EMEX mesoscale precipitation feature properties and their environmental characteristics. *Mon. Wea. Rev.,* **120,** 554–564.

Barnes, G. M., and K. Sieckman, 1984: The environment of fast- and slow-moving tropical mesoscale convective cloud lines. *Mon. Wea. Rev.,* **112,** 1782–1794.

Blanchard, D. O., 1990: Mesoscale convective patterns of the southern high plains. *Bull. Amer. Meteor. Soc.,* **71,** 994–1005.

Brandes, E. A., 1984: Relationships between radar-derived thermodynamic variables and tornadogenesis. *Mon. Wea. Rev.,* **112,** 1033–1052.

Caniaux, G., J.-P. Lafore, and J.-L. Redelsperger, 1995: A numerical study of the stratiform region of a fast-moving squall line. Part II: Relationship between mass, pressure, and momentum fields. *J. Atmos. Sci.,* **52,** 331–352.

Chen, S. S., R. A. Houze Jr., and B. E. Mapes, 1996: Multiscale variability of deep convection in relation to large-scale circulation in TOGA COARE. *J. Atmos. Sci.,* **53,** 1380–1409.

Davis, C. A., and M. L. Weisman, 1994: Balanced dynamics of mesoscale vortices produced in mesoscale convective systems. *J. Atmos. Sci.,* **51,** 2005–2030.

Dudhia, J., and M. W. Moncrieff, 1987: A numerical simulation of quasi-stationary tropical convective bands. *Quart. J. Roy. Meteor. Soc.,* **113,** 929–967.

Fritsch, J. M., and R. A. Maddox, 1981: Convectively driven mesoscale convective systems aloft. Part I: Observations. *J. Appl. Meteor.,* **20,** 9–19.

Fujita, T. T., 1978: Manual of downburst identification for Project Nimrod. Satellite and Mesometeorology Research Paper 156, Department of Geophysical Sciences, University of Chicago, Chicago, IL, 104 pp.

Gallus, W. A., and R. H. Johnson, 1992: The momentum budget of an intense midlatitude squall line. *J. Atmos. Sci.,* **49,** 422–450.

Gao, K., D.-L. Zhang, M. W. Moncrieff, and H.-R. Cho, 1990: Mesoscale momentum budget in a midlatitude squall line: A numerical case study. *Mon. Wea. Rev.,* **118,** 1011–1028.

Hane, C. E., and D. P. Jorgensen, 1995: Dynamic aspects of a distinctly three-dimensional mesoscale convective system. *Mon. Wea. Rev.,* **123,** 3194–3214.

Houze, R. A., Jr., 1993: *Cloud Dynamics.* Academic Press, 573 pp.

——, B. F. Smull, and P. Dodge, 1990: Mesoscale organization of springtime rainstorms in Oklahoma. *Mon. Wea. Rev.,* **118,** 613–654.

Johnson, R. H., 1980: Diagnosis of convective and mesoscale motions during phase III of GATE. *J. Atmos. Sci.,* **37,** 733–753.

Jorgensen, D. P., B. F. Smull, S. Lewis, and M. A. LeMone, 1996: Structure and momentum fluxes of four TOGA-COARE convective systems observed by airborne Doppler radar. Preprints, *Seventh Conf. on Mesoscale Processes,* Reading, United Kingdom, Amer. Meteor. Soc. and Roy. Meteor. Soc., 295–297.

——, M. A. LeMone, and S.B. Trier, 1997: Structure and evolution of the 22 February 1993 TOGA-COARE squall line: Observations of precipitation, circulation, and surface energy fluxes. *J. Atmos. Sci.,* **54,** 1961–1985.

Kiladis, G. N., G. A. Meehl, and K. M. Weickmann, 1994: Large-scale circulation associated with westerly wind bursts and deep convection over the western equatorial Pacific. *J. Geophys. Res.,* **99,** 18 527–18 544.

Klemp, J. B., and R. Rotunno, 1983: A study of the tornadic region within a supercell thunderstorm. *J. Atmos. Sci.,* **40,** 359–377.

Lafore, J.-P., J.-L. Redelsperger, and G. Jaubert, 1988: Comparison between a three-dimensional simulation and Doppler radar data of a tropical squall line: Transports of mass, momentum, heat, and moisture. *J. Atmos. Sci.,* **45,** 3483–3500.

LeMone, M. A., 1983: Momentum transport by a line of cumulonimbus. *J. Atmos. Sci.,* **40,** 1815–1834.

——, and D. P. Jorgensen, 1991: Precipitation and kinematic structure of an oceanic mesoscale convective system. Part II: Momentum transport and generation. *Mon. Wea. Rev.,* **119,** 2638–2653.

——, and M. W. Moncrieff, 1994: Momentum and mass transport by convective bands: Comparisons of highly idealized dynamical models to observations. *J. Atmos. Sci.,* **51,** 281–305.

——, G. M. Barnes, and E. J. Zipser, 1984: Momentum fluxes by lines of cumulonimbus over the tropical oceans. *J. Atmos. Sci.,* **41,** 1914–1932.

——, E. J. Zipser, and S. B. Trier, 1998: The role of environmental shear and thermodynamic conditions in determining the structure and evolution of mesoscale convective systems during TOGA COARE. *J. Atmos. Sci.,* in press.

Lin, X., and R. H. Johnson, 1996: Kinematic and thermodynamic characteristics of the flow over the western Pacific warm pool during TOGA COARE. *J. Atmos. Sci.,* **53,** 695–715.

Lin, Y.-J., T.-C. C. Wang, R. Pasken, and Z.-S. Deng, 1990: Characteristics of a subtropical squall line determined from TAMEX dual-Doppler data. Part II: Dynamic and thermodynamic structures and momentum budgets. *J. Atmos. Sci.,* **47,** 2382–2399.

Loehrer, S. M., and R. H. Johnson, 1995: Surface pressure and precipitation life cycle characteristics of PRE-STORM mesoscale convective systems. *Mon. Wea. Rev.,* **123,** 600–621.

Madden, R. A., and P. R. Julian, 1972: Description of global-scale circulation cells in the tropics with a 40–50 day period. *J. Atmos. Sci.,* **29,** 1109–1123.

——, and ——, 1994: Observations of the 40–50-day tropical oscillation—A review. *Mon. Wea. Rev.,* **122,** 814–837.

Moncrieff, M. W., 1981: A theory of organized steady convection and its transport properties. *Quart. J. Roy. Meteor. Soc.,* **107,** 29–50.

——, 1992: Organised mesoscale convective systems: Archetypal dynamical models, mass and momentum flux theory, and parameterization. *Quart. J. Roy. Meteor. Soc.,* **118,** 819–850.

Newton, C. W., 1950: Structure and mechanism of the prefrontal squall line. *J. Meteor.,* **7,** 210–222.

Rickenbach, T. M., and S. A. Rutledge, 1998: Convection in TOGA COARE: Horizontal scale, morphology, and rainfall production. *J. Atmos. Sci.,* **55,** 2715–2729.

Rotunno, R., J. B. Klemp, and M. L. Weisman, 1988: A theory for strong, long-lived squall lines. *J. Atmos. Sci.,* **45,** 463–485.

Rutledge, S. A., and P. V. Hobbs, 1984: The mesoscale and microscale structure and organization of clouds and precipitation in midlatitude cyclones. Part XII: A diagnostic modeling study of precipitation in narrow cold-frontal rainbands. *J. Atmos. Sci.,* **41,** 2949–2972.

Skamarock, W. C., 1989: Truncation error estimates for refinement criteria in nested and adaptive models. *Mon. Wea. Rev.,* **117,** 882–886.

——, and J. B. Klemp, 1993: Adaptive grid refinement for two-dimensional and three-dimensional nonhydrostatic atmospheric flow. *Mon. Wea. Rev.,* **121,** 788–804.

——, M. L. Weisman, and J. B. Klemp, 1994: Three-dimensional evolution of simulated long-lived squall lines. *J. Atmos. Sci.,* **51,** 2563–2584.

Smull, B. F., and R. A. Houze Jr., 1987: Dual-Doppler radar analysis of a midlatitude squall line with a trailing region of stratiform rain. *J. Atmos. Sci.,* **44,** 2128–2148.

——, and J. A. Augustine, 1993: Multiscale analysis of a mature mesoscale convective complex. *Mon. Wea. Rev.,* **121,** 103–132.

Tao, W.-K., and J. Simpson, 1989: Modeling study of a squall-type convective line. *J. Atmos. Sci.,* **46,** 177–202.

Trier, S. B., 1997: Multiscale analysis of a simulated oceanic MCS and its environmental impact. NCAR Cooperative Thesis 162, 241 pp. [Available from National Center for Atmospheric Research, P.O. Box 3000, Boulder, CO 80307.]

——, W. C. Skamarock, M. A. LeMone, D. B. Parsons, and D. P. Jorgensen, 1996: Structure and evolution of the 22 February 1993 TOGA-COARE squall line: Numerical simulations. *J. Atmos. Sci.,* **53,** 2861–2886.

——, ——, and ——, 1997: Structure and evolution of the 22 February 1993 TOGA COARE squall line: Organization mechanisms inferred from numerical simulation. *J. Atmos. Sci.,* **54,** 386–407.

Webster, P. J., and R. Lukas, 1992: TOGA COARE: The Coupled Ocean–Atmosphere Response Experiment. *Bull. Amer. Meteor. Soc.,* **73,** 1377–1416.

Weisman, M. L., 1992: The role of convectively generated rear-inflow jets in the evolution of long-lived mesoconvective systems. *J. Atmos. Sci.,* **49,** 1827–1847.

——, 1993: The genesis of severe long-lived bow-echoes. *J. Atmos. Sci.,* **50,** 645–670.

——, and J. B. Klemp, 1986: Characteristics of isolated convective storms. *Mesoscale Meteorology and Forecasting,* P. Ray, Ed., Amer. Meteor. Soc., 390–413.

Weller, R. A., and S. P. Anderson, 1996: Surface meteorology and air–sea fluxes in the western equatorial Pacific warm pool during the TOGA Coupled Ocean–Atmosphere Response Experiment. *J. Climate,* **9,** 1959–1990.

Yang, M.-J., and R. A. Houze Jr., 1996: Momentum budget of a squall line with trailing stratiform precipitation: Calculations with a high-resolution numerical model. *J. Atmos. Sci.,* **53,** 3629–3652.

Young, G. S., S. M. Perugini, and C. W. Fairall, 1995: Convective wakes in the equatorial western Pacific during TOGA. *Mon. Wea. Rev.,* **123,** 110–123.

Zipser, E. J., 1977: Mesoscale and convective-scale downdrafts as distinct components of squall line structure. *Mon. Wea. Rev.,* **105,** 1568–1589.